to gain insight into the quenching mechanism and the reasons for its inefficiency in the case of the phosphonate ligands.

Acknowledgment. This research was supported by a grant from the National Science Foundation (CHEM-8821707). We wish to thank Brian Herr for assistance with some of the measurements, Drs. Charles McNemar and Patrick Breen for writing portions of the computer code used in this study, and Dr. Richard Holz for helpful discussions.

Registry No. ATP, 56-65-5; Ce^{3+}, 18923-26-7; Eu^{3+}, 22541-18-0; Tb^{3+}, 22541-20-4; tubercidin, 69-33-0.

Contribution from the Department of Chemistry, Texas A&M University, College Station, Texas 77843-3255

Nature of Metal–Metal Interactions in Systems with Bridging Ligands. 1. Electronic Structure and Bonding in Octacarbonyldicobalt

Arthur A. Low, Kathryn L. Kunze, P. J. MacDougall, and Michael B. Hall*

Received October 9, 1990

Self-consistent field calculations on $Co_2(CO)_8$ were used to examine its electronic structure through an analysis of the electron density. In the standard deformation density map, an accumulation zone extends from the cobalt nucleus toward the region of the Co–Co bent bond. This accumulation in the Co–Co bent-bond region is rather weak and could be due to coincidental accumulations in the vacant coordination site of each cobalt. However, through the use of various promolecules to produce different fragment deformation density maps, it can be concluded that the accumulation of density in the bent-bond region must be due at least in part to constructive interference between the two cobalt atoms. An analysis of the topology of the charge density of $Co_2(CO)_8$ shows interaction lines between the Co atoms and the C atoms with (3,−1) critical points, which are indicative of a bond. There is no interaction line connecting the Co atoms. Instead, there is a (3,+1) ring critical point close to the Co–Co midpoint. Therefore, although some constructive interference occurs between the two cobalt atoms, it is not sufficient to produce a Co–Co bond in the topology of the charge density.

Introduction

Early descriptions of the bonding in the bridged isomer of $Co_2(CO)_8$ (**1**), which is the most stable isomer in the solid state,

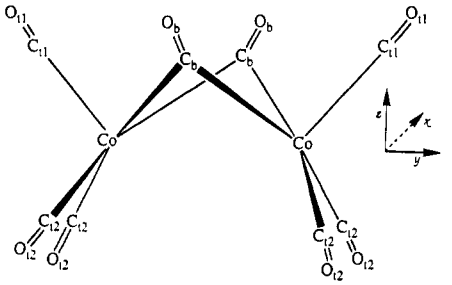

1

assumed the 18e⁻ rule, which requires a Co–Co single bond.[1] The main argument at that time was whether the Co–Co bond was bent, **2**, or straight, **3**.

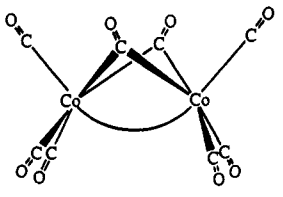

2

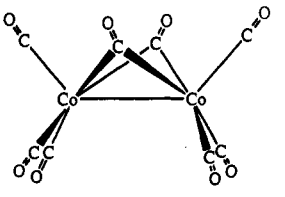

3

Subsequent molecular orbital calculations at the extended Hückel level suggested that it was not necessary to postulate any direct Co–Co bond.[2,3] These calculations supported a model in which all of the bonding between the cobalt atoms occurred through the carbonyl bridges. However, the results of molecular orbital calculations using the CNDO formalism yielded a bond between the cobalt atoms.[4]

In hope of providing some direct experimental evidence on the metal–metal interaction in $Co_2(CO)_8$, Leung and Coppens determined the experimental deformation density of $Co_2(CO)_8$.[5] Unfortunately, their deformation density maps yielded no features that could definitely be attributed to any Co–Co bond either bent or straight. This is not a terribly surprising result, since even in the experimental deformation density of $Mn_2(CO)_{10}$, in which there is definitely a Mn–Mn bond, the accumulation region in the Mn–Mn internuclear region is below the estimated standard deviation of the crystal structure analysis.[6]

The lack of sizeable accumulation in the Mn–Mn internuclear region in the experimental deformation density of $Mn_2(CO)_{10}$ can be attributed to the inappropriate choice of the spherical atom promolecule. In the case of $Mn_2(CO)_{10}$, a more appropriate choice of promolecule is the sum of the density of two properly oriented 17-electron $Mn(CO)_5$ fragments. When a theoretical deformation density of $Mn_2(CO)_{10}$ is computed with this promolecule, the resultant maps show a significant accumulation between the Mn atoms.[7] Perhaps a more appropriate promolecule of fragment densities can be chosen for $Co_2(CO)_8$, which could more clearly show the interaction between the two Co fragments.

There have been theoretical deformation density studies based on discrete variational X-α calculations for the dinuclear metal carbonyls $Mn_2(CO)_{10}$, $Fe_2(CO)_9$, and $Co_2(CO)_8$.[8] The resultant maps showed an internuclear accumulation between the Mn atoms for $Mn_2(CO)_{10}$, but no accumulation regions associated with a M–M bond could be found in the maps of either $Fe_2(CO)_9$ or $Co_2(CO)_8$. Theoretical and experimental deformation density studies have been performed for the dinuclear metal compounds $[(\eta^5\text{-}C_5H_5)Fe(CO)_2]_2$[9,10] and $Co_2(CO)_6(\mu_2\text{-}RCCR)$.[11] No evi-

(1) Braterman, P. S. *Struct. Bonding (Berlin)* **1972**, *10*, 57.
(2) Thorn, D. L.; Hoffmann, R. *Inorg. Chem.* **1978**, *17*, 126.
(3) Summerville, R. H.; Hoffmann, R. *J. Am. Chem. Soc.* **1979**, *101*, 3821.
(4) (a) Freund, H.-J.; Hohlneicher, G. *Theoret. Chim. Acta (Berlin)* **1979**, *51*, 145. (b) Freund, H.-J.; Dick, B.; Hohneicher, G. *Theoret. Chim. Acta (Berlin)* **1980**, *57*, 181.
(5) Leung, P. C.; Coppens, P. *Acta Crystallogr., Sect. B* **1983**, *B39*, 535.
(6) Martin, M.; Rees, B.; Mitschler, A. *Acta Crystallogr., Sect. B* **1982**, *B38*, 6.
(7) Hall, M. B. In *Electron Distributions and the Chemical Bond*; Coppens, P., Hall, M. B., Eds.; Plenum: New York, 1982; p 205.
(8) Heijser, W.; Baerends, E. J.; Ros, P. *Faraday Symp. Chem. Soc.* **1980**, *14*, 211.

0020-1669/91/1330-1079$02.50/0

dence for a direct Fe–Fe bond could be found in either experimental or theoretical deformation density maps of the iron compound. However, the theoretical deformation density of the dicobalt complex suggested the presence of a bent Co–Co bond. An ab initio SCF study has been performed for $Fe_2(CO)_9$ in which no evidence of a direct Fe–Fe bond could be found.[12] As of yet, an ab initio SCF study of $Co_2(CO)_8$ has not been reported in the literature.

The topological analysis of the charge density is another method used to examine the bonding in various molecules.[13] From this analysis, a necessary and sufficient condition for the existence of a bond between two neighboring atoms is the presence of a bond path between the two atoms. A preliminary topological study on dinuclear metal carbonyls[14] shows a bond path connecting the Mn atoms in $Mn_2(CO)_{10}$. A particular advantage that this analysis has over deformation density studies is the absence of an arbitrary reference point such as a promolecule. This study is the first use of this analysis on dinuclear carbonyls with bridging ligands.

In this work, the nature of the Co–Co interaction in $Co_2(CO)_8$ will be examined through the use of deformation density studies and a topological analysis of the total density both derived from an ab initio SCF wave function. Besides the spherical atom promolecule, we will utilize two different promolecules consisting of the densities of fragments representing the bonded and nonbonded states of $Co_2(CO)_8$. Consideration of all these maps should shed some light on the nature of the metal–metal interaction in $Co_2(CO)_8$.

Theoretical Methods

The molecular orbitals were generated via the closed-shell Hartree–Fock–Roothaan method.[15] The geometry of the molecule was taken from the low-temperature crystal structure analysis reported in the deformation density study of $Co_2(CO)_8$.[5] The geometry was idealized to give the molecule overall C_{2v} symmetry. The Gaussian basis sets used were Huzinaga's (13s7p5d/4s3p3d) basis for Co[16] with an additional p function, whose exponent is one-third of the formerly most diffuse p function, and Huzinaga's (6s3p/3s2p) basis for the C and O atoms.[16]

A number of different deformation density maps were computed by subtracting various promolecules from the total electron density of the molecule. For the standard deformation density, the promolecule consisted of the sum of the densities of the spherically averaged cobalt (s^2d^7), carbon, and oxygen atoms. Two different fragment deformation densities were calculated from promolecules that represent the fragments immediately prior to molecular formation in either the "nonbonded" form or the "bonded" form of $Co_2(CO)_8$. Both of these promolecules will be discussed in more detail later.

The deformation density plots, except for those in Figure 2, are contoured geometrically with each contour differing by a factor of 2. Negative contours are dashed. The absolute value of the smallest contour is 0.01 e Å^{-3}. The deformation density plots in Figure 2 are contoured as the experimental maps with linear contours at a contour interval of 0.1 e Å^{-3}. The molecular orbital plots are contoured geometrically as before, but the absolute value of the smallest contour now has a value of $\pm 2^{-7}$ (e (au)$^{-3}$)$^{1/2}$.

The topology of the charge density of $Co_2(CO)_8$ was studied in order to determine whether charge is locally concentrated or depleted in the internuclear regions.[13,17] This analysis utilizes both the gradient ($\nabla\rho$) and the Laplacian ($\nabla^2\rho$) of the charge density. Points at which $\nabla\rho = 0$ are called critical points. According to this analysis, all atoms in a molecule are each bounded by a zero-flux surface. The area enclosed by a particular atom's zero-flux surface is called its basin. A necessary

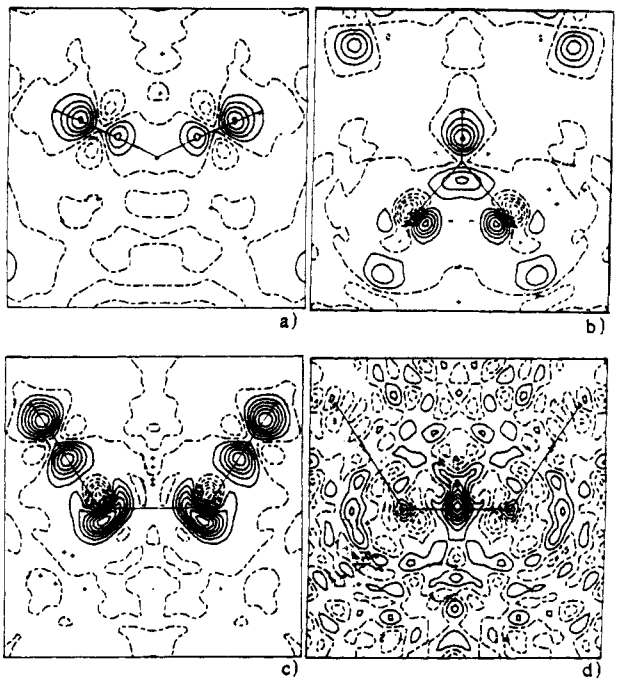

Figure 1. Experimental deformation density maps from low-temperature structural analysis of $Co_2(CO)_8$ by Leung and Coppens.[4] The deformation density after multipole refinement are shown in (a) the plane containing the bridging carbonyls, (b) the plane containing the two cobalt atoms and one of the bridging carbonyls, and (c) the plane containing the two cobalt atoms and the axial terminal carbonyls. The residual density is shown in the plane of the two cobalt atoms and the two axial terminal carbonyls in (d). The maps are contoured linearly with a contour interval of 0.10 e Å^{-3}. Negative contours are dashed.

requirement for the existence of a bond between two atoms is that there be an atomic interaction line called a bond path on which the density is a maximum in all directions perpendicular to this line. Where this bond path crosses the zero-flux surface between the two atoms, a (3,−1) bond critical point exists. Atomic nuclei, which are local maxima of charge density, correspond to (3,−3) critical points. There are two more types of stable critical points in three dimensional space: (3,+1) ring critical points and (3,+3) cage critical points. A (3,+1) ring critical point exists at the point of minimum charge density inside a ring of atoms. Charge density is a minimum in the ring surface at a (3,+1) critical point and a maximum in the direction perpendicular to the ring. For example, a (3,+1) critical point exists inside each ring of the [2.2.2]propellane molecule.[18] A (3,+3) cage critical point exists at the point of minimum charge density inside a cage of atoms. Charge density is a minimum in all directions at a (3,+3) critical point. For example, a (3,+3) cage critical point can be found between the bridgehead carbon atoms in the bicyclo[1.1.1]pentane molecule.[18]

The existence of a bent or straight bond in $Co_2(CO)_8$, if it exists, should also be revealed by the topological analysis. In the analysis of strained organic systems, such as cyclopropane, the bond paths between the strained carbon–carbon bonds were bent outside the C–C internuclear axes that form the C_3 ring.[19] It follows that if a bent bond exists in $Co_2(CO)_8$, it should be reflected in the bond path between the two cobalt atoms.

The gradient vector field of $\rho(r)$ for $Co_2(CO)_8$ is plotted in the planes of symmetry of the molecule. All gradient paths originate and terminate at critical points where $\nabla\rho = 0$. In these plots, there are 24 paths terminating at each (3,−3) critical point, or at each nucleus. For each (3,−1) critical point, there are paths that originate from ∞ and terminate at the critical point, approaching perpendicularly to the bond axis, as well as two unique paths originating at the critical point and terminating at the neighboring nuclei.

The molecular orbital calculations were performed with the GAMESS package of programs.[20] All molecular orbital density plots and plots

(9) Mitschler, A.; Rees, B.; Lehmann, M. S. *J. Am. Chem. Soc.* **1978**, *100*, 3390.
(10) Benard, M. *J. Am. Chem. Soc.* **1978**, *100*, 7740.
(11) Baert, F.; Guelzim, A.; Poblet, J. M.; Wiest, R.; Demuynck, J.; Benard, M. *Inorg. Chem.* **1986**, *25*, 1830.
(12) Bauschlicher, C. W. *J. Chem. Phys.* **1986**, *84*, 872.
(13) (a) Bader, R. F. W.; Nguyen-Dang, T. T.; Tal, Y. *Rep. Prog. Phys.* **1981**, *44*, 893. (b) Bader, R. F. W.; Essen, H. *J. Chem. Phys.* **1984**, *80*, 1943.
(14) MacDougall, P. J. Ph.D. Thesis, Department of Chemistry, McMaster University, Hamilton, Ontario, Canada, 1989.
(15) Roothaan, C. C. J. *Rev. Mod. Phys.* **1951**, *23*, 69.
(16) Huzinaga, S., Ed. In *Gaussian Basis Sets for Molecular Calculations*; Elsevier Science Publishers: New York, 1984.
(17) Bader, R. F. W.; MacDougall, P. J.; Lau, C. D. H. *J. Am. Chem. Soc.* **1984**, *106*, 1594.
(18) Bader, R. F. W. *Acc. Chem. Res.* **1985**, *18*, 9.
(19) (a) Runtz, G. R.; Bader, R. F. W.; Messer, R. R. *Can. J. Chem.* **1977**, *55*, 3040. (b) Wiberg, K. B.; Bader, R. F. W.; Lau, C. D. H. *J. Am. Chem. Soc.* **1987**, *109*, 985.
(20) M. F. Guest, SERC Daresbury Laboratory, Warrington, U.K., provided GAMESS version 4.0.

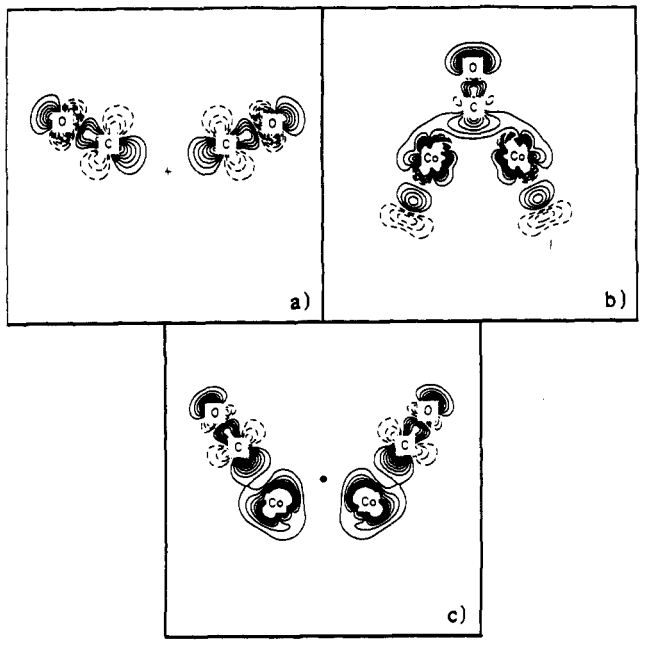

Figure 2. Calculated deformation density maps of $Co_2(CO)_8$. The deformation density is shown in (a) the plane containing the bridging carbonyls (the xz plane) (the projection of the Co–Co axis denoted by a "+", (b) the plane containing the two cobalt atoms and one of the bridging carbonyls (the $Co_2(\mu$-C) plane), and (c) the plane containing the two cobalt atoms and the axial terminal carbonyls (the *yz* plane) (the projection of the bridging carbon atoms denoted by a "+"). The contouring scheme is the same as in the experimental maps.

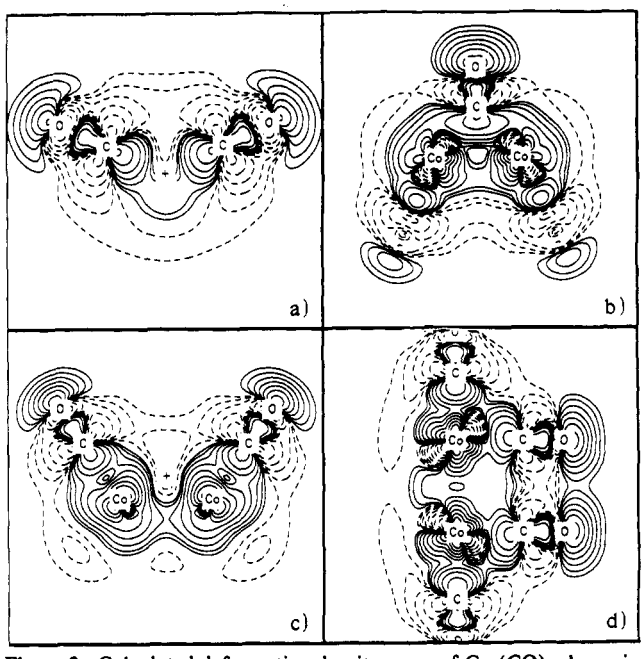

Figure 3. Calculated deformation density maps of $Co_2(CO)_8$ shown in the same planes as in Figure 2 but with geometric contours with each contour differing by a factor of 2. The absolute value of the smallest contour is 0.01 e Å^{-3}. The deformation density map shown in (d) is for the unbridged D_{3h} isomer of $Co_2(CO)_8$ in one of the diagonal planes containing the cobalt atoms and two of the equatorial terminal carbonyls and the axial terminal carbonyls.

involving the topological analysis were made by using an interactive version of MOPLOT.[21]

Results and Discussion

Deformation Density Plots. The experimental deformation density maps from Coppens' study[5] are shown in Figure 1. The theoretical deformation density maps are shown in Figure 2. Both are linearly contoured with a contour interval of 0.1 e Å^{-3}. It must be noted beforehand that the experimental maps contain the effects of thermal motion whereas the theoretical maps are static. Figures 1a and 2a show the deformation density in a plane containing the bridging carbonyls perpendicular to the Co–Co axis (or the *xz* axis in our calculations). Accumulations in the carbon lone-pair region and along the C–O bond axis as well as deficit in the carbon π region can clearly be observed in both maps. The accumulation region due to formation of the oxygen lone pair and deficit region in the π region about the O atoms, which are clearly seen in the theoretical maps, are not seen in the experimental maps apparently because of the effects of thermal smearing and libration of the O atom. The lack of features about the O atom in the experimental deformation density maps of carbonyl is a common occurrence.[22]

Figures 1b and 2b show the deformation density in the plane containing one of the bridging carbonyls and both cobalt atoms. The spreading of the carbon lone-pair density can be clearly seen in both maps. As in the previous plot, the features about the O atom do not appear in the experimental maps. The deficit in the π regions of CO is now much smaller than in the perpendicular plane indicative of greater π back-donation to the in-plane 2π orbital. The pattern about the Co atom shows deficit along the $Co–C_{br}$ axis due at least in part to π back-donation to the bridging carbonyl. The remaining features about the cobalt atom in the theoretical maps show a quadrifid accumulation pattern in which two lobes point along the Co–Co axis and the remaining two lobes point along a line where one might expect a bent Co–Co bond. The latter lobes are in the same direction as the polarization of the metal density in the experimental map.

Figures 1c and 2c show the deformation density containing both cobalt atoms and the axial terminal carbonyls (or the *yz* plane in our calculation). One would expect this plane to contain the bent Co–Co bond if it exists. The same differences between the experimental and theoretical maps about the carbonyls in the earlier maps can be observed about the terminal carbonyls in these maps. The two maps really differ near the Co atom. In the theoretical map, there is a small deficit region along the $Co–C_t$ axis that is partially swamped by a bilobed accumulation region, which roughly points toward the projection of the bridging C atom in this plane (denoted by a "+" in the map). This accumulation can be attributed to "crystal-field" effects, which removes density, relative to the spherical atom, from the metal orbitals pointing toward the ligands and places it in the orbitals pointing between the ligands. There is not a large polarization of the metal density toward the bent-bond region, as seen in the experimental maps. However, the contours of the large accumulation region do deform in the direction of the Co–Co bent bond.

Figure 1d shows the residual density in the plane containing the two cobalt atoms and the axial terminal carbonyls. The accumulation near the Co–Co midpoint can clearly be observed. The sharpness of this peak, which is not what would be expected from the constructive interference of metal d orbitals, as well as the absence of any such peaks in the early theoretical deformation density maps,[8] led the authors of the experimental study to suggest that this peak was due to an accumulation of experimental error. Our maps support that conclusion.

In order to better examine the nature of any direct Co–Co interaction, the theoretical maps were replotted with geometric contours where the absolute value of the smallest contour now equals 0.01 e Å^{-3}. These maps are shown in Figure 3. Figure 3a, again showing the deformation density in the *xz* plane, shows a diffuse accumulation region centered below the Co–Co axis (indicated by a "+" in the plot). This region can also clearly be observed in Figure 3c, which shows the deformation density in the *yz* plane. What may at first glance appear to be a separate

(21) Interactive MOPLOT: a package for the interactive display and analysis of molecular wave functions incorporating the programs MOPLOT (D. Lichtenburger), PLOTDEN (R. F. W. Bader, D. J. Kenworthy, P. M. Beddall, G. R. Runtz, and S. G. Anderson), SCHUSS (R. F. W. Bader, G. R. Runtz, S. G. Anderson, and F. W. Biegler-Koenig), and EXTREM (R. F. W. Bader and F. W. Biegler-Koenig) written by P. Sherwood and P. J. MacDougall, 1989.

(22) Hall, M. B. *Chem. Scr.* **1986**, *26*, 389.

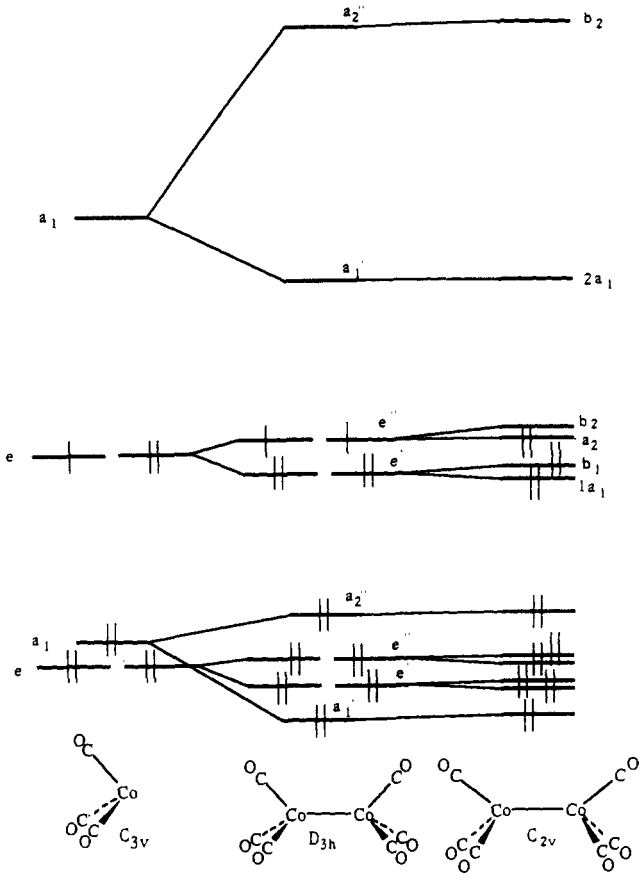

Figure 4. Qualitative molecular orbital diagram from the formation of the C_{2v} form of $Co_2(CO)_6$ from two $Co(CO)_3$ fragments.

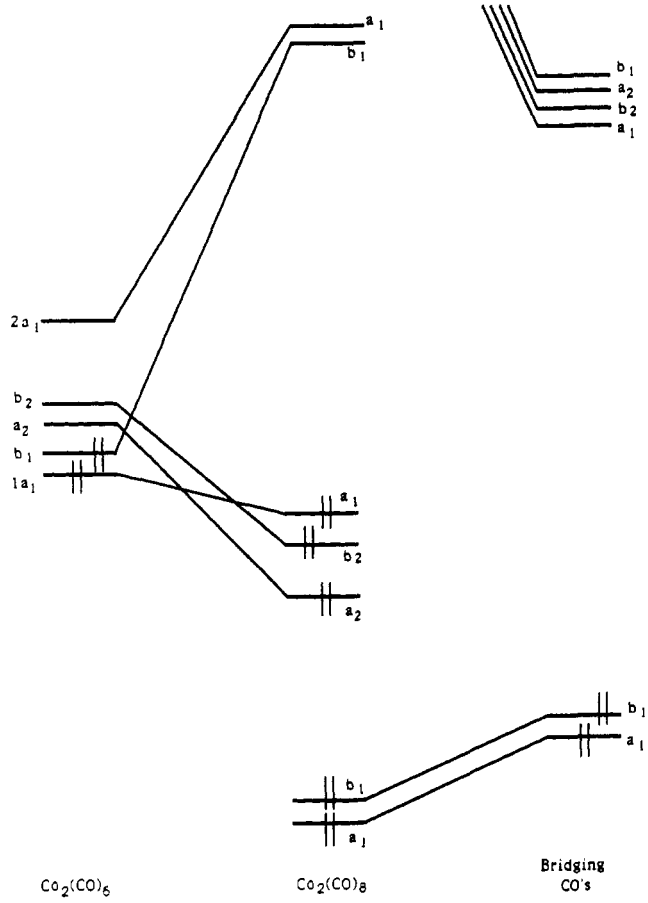

Figure 5. Qualitative molecular orbital diagram of the formation of $Co_2(CO)_8$ from a $Co_2(CO)_6$ fragment and two bridging carbonyls.

accumulation region between the Co and carbon lone-pair accumulation region is actually a region of lower accumulation and is probably due to the swamping out of the loss of density in the orbital pointing toward the terminal carbonyl by the accumulation region pointing toward the projection of the bridging carbon atom. The same thing happens in Figure 3b in the region between the bridging carbon's lone-pair accumulation region and the two cobalt atoms where there are enclosed contours of lower accumulation than in the surrounding area.

The accumulation region in the anticipated bent-bond region of the cobalt atoms appears as a saddle point between the contours of accumulation about the cobalt atoms. This is in contrast to the accumulation peaks along the Co–Co midpoint in the deformation density map of the unbridged D_{3h} isomer of $Co_2(CO)_8$ shown in Figure 3d. The accumulation peak in Figure 3d is located at the midpoint of the Co–Co axis and has an accumulation of density which is approximately 3 times larger than that at the midpoint of the Co–Co bent-bond accumulation region in Figure 3c.

The difference between the shape of the internuclear Co–Co accumulation in the deformation density maps of the C_{2v} isomer and that of the D_{3h} isomer points out that the Co–Co interaction is different in the two isomers. Also, the small size and the shape of the accumulation region in the Co–Co bent-bond region in Figure 3c suggests that it may not be due to constructive interference but to overlapping accumulations in the vacant coordination sites on each cobalt atom.

Orbital Analysis. The qualitative description of the orbitals obtained from our ab initio calculation is similar to the description of Thorn and Hoffmann.[2] The MO diagrams shown in Figures 4 and 5 are constructed from our approximate Fenske–Hall[23] calculations on the formation of $Co_2(CO)_8$ from two $Co(CO)_3$ fragments and two CO molecules. The results are quite similar to the MO diagrams of Thorn and Hoffmann.[2]

The description starts with a $Co(CO)_3$ fragment. The three terminal carbonyls split the 3d orbitals into a t_{2g}-like set (the a_1 and lower e set) and an e_g-like set (the higher lying e set). At somewhat higher energy is an a_1 orbital that contains substantial 4s and 4p character. As two $Co(CO)_3$ fragments interact to form the D_{3h} dimer $Co_2(CO)_6$, the molecular orbitals interact as shown in the center column of Figure 4. In forming $Co_2(CO)_6$, the t_{2g}-like orbitals interact to form six low-lying filled orbitals. The e_g-like orbitals form a M–M π-bonding e′ set and a M–M π^*-antibonding e″ set. The a_1 orbitals combine to form a bonding and antibonding orbital of σ-type symmetry, a_1' and a_2'', respectively.

In preparation to form the $Co_2(CO)_8$ molecule, the $Co(CO)_3$ fragments need to tilt so that their 3-fold axes no longer align with the M–M axis. This reduces the symmetry of the $Co_2(CO)_6$ fragment to C_{2v} and modifies the molecular orbitals, as shown on the right side of Figure 4. The π-bonding e′ set splits into the a_1 and b_1 orbital; the π-antibonding e″ set splits into the a_2 and b_2 orbital. The fragment orbitals derived from the a_1 hybrid both rise in energy to form the $2a_1$ and b_2 orbitals.

The interaction of the $Co_2(CO)_6$ fragment with the two bridging carbonyls is shown in Figure 5. Only the fragment orbitals primarily involved in the interaction are shown on the left-hand side of the diagram. The bridging carbonyls' 5σ and 2π orbital combinations are shown on the right-hand side of the diagram. The carbonyls' 5σ orbitals transform as a_1 and b_1, while the 2π orbitals transform as a_1, b_1, b_2, and a_2. The 5σ orbitals interact with the dimer's b_1 and $2a_1$ orbitals raising the energy of the metal orbitals. The strongest interaction is with the $2a_1$ orbital. The strongest interactions of the carbonyls' 2π orbitals are with the metal dimer's b_2 and a_2 orbitals. The a_1 orbital that was initially a π-bonding orbital in the nontilted D_{3h} $M_2(CO)_6$ fragment is now the bent M–M σ-bonding orbital. The ab initio calculation results in the same orbital occupancy as shown in Figure 6 even if the order of the upper orbitals may be interchanged. For our purposes, the absolute order of the orbitals is not important as long as the proper orbitals are filled.

(23) Hall, M. B.; Fenske, R. F. *Inorg. Chem.* **1972**, *11*, 768.

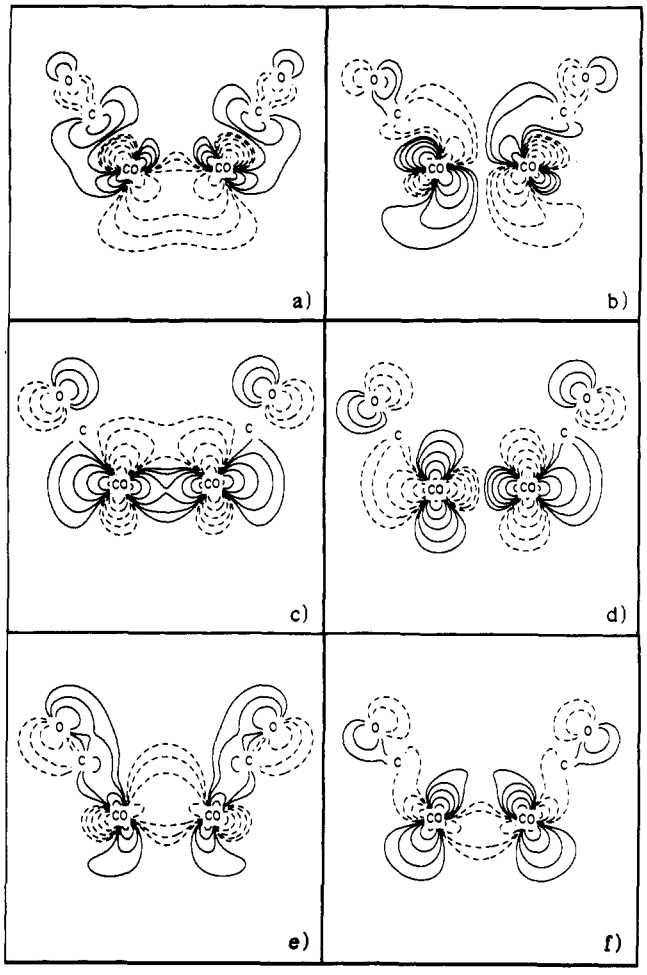

Figure 6. Molecular orbital plots of (a) the metal–metal bonding a_1 "e_g-like" orbital, (b) the metal–metal antibonding b_2 "e_g-like" orbital, (c) the metal–metal bonding "t_{2g}-like" a_1 orbital, and (d) the metal–metal antibonding "t_{2g}-like" b_2 orbital. (e) and (f) show the metal character of the two a_1 orbitals that possess the primary bridging carbonyl 5σ to metal donations. All plots are in the *yz* plane and are contoured geometrically with each contour differing by a factor of 2. The absolute value of the smallest contour is 2^{-6} (0.015 63) (e au^{-3})$^{1/2}$.

For the C_{2v} point group, the subscript symmetry labels 1 and 2 refer to symmetry with respect to the plane containing the bridging carbonyls, or the *xz* plane. Subscript 1 is symmetric with respect to this plane, thus the orbital is metal–metal bonding, while subscript 2 is antisymmetric, thus the orbital is metal–metal antibonding. Among the three highest occupied MO's, there are two metal–metal antibonding (a_2 and b_2) and one metal–metal (a_1) bonding orbitals. Therefore, if one only considers the three high-lying frontier orbitals, the net result would be a net metal–metal antibonding interaction. The net constructive interference, if any, must come from the remaining orbitals.

Several of the molecular orbitals of $Co_2(CO)_8$ are plotted in Figure 6. Parts a and b of Figure 6 show the high-lying metal–metal bonding a_1 orbital and metal–metal antibonding b_2 orbital, respectively, in the plane containing the cobalt atoms and the terminal axial carbonyls (the *yz* plane). The other high-lying frontier orbital, a_2, has a node in this plane. Examination of the metal–metal interaction by counting contour levels shows that the bonding interaction in the a_1 orbital is nearly cancelled by the antibonding interaction in the b_2 orbital.

Parts c and d of Figure 6 show two of the six MO's that derive from the in-phase and out-of-phase combinations of the t_{2g}-like orbitals. The back-bonding to the terminal carbonyls can clearly be seen in these plots. Previous work[24] on larger clusters (with 3rd row transition metals and approximate molecular orbital calculations) has suggested that the in-phase combination might have more metal character while the out-of-phase combination might have more carbonyl character, a situation that could result in a net-attractive interaction between the metals. However, here there is again near cancellation of metal–metal bonding and antibonding contributions.

(24) Sherwood, D. E.; Hall, M. B. *Inorg. Chem.* **1982**, *21*, 3458.

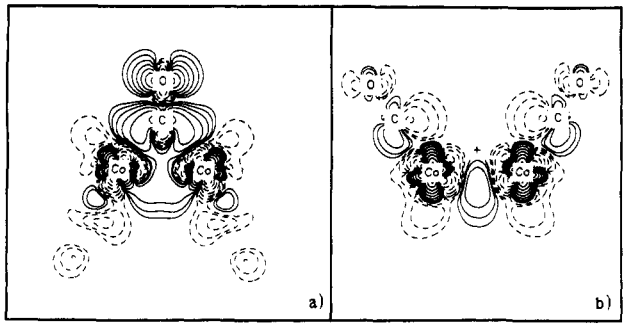

Figure 7. "Nonbonded" fragment deformation density maps of $Co_2(CO)_8$ with a promolecule of the sum of the densities of two isolated doublet $Co(CO)_3$ fragments and two isolated ground-state CO molecules in the same geometry as the parent molecule. The maps are shown in (a) the $Co_2(\mu\text{-}C)$ plane and (b) the *yz* plane. The contouring scheme is the same as that in Figure 3.

The next orbitals to consider are the filled carbonyls' 5σ a_1 and b_1 orbitals. The b_1 orbitals possess a node in the *yz* plane and therefore will not contribute density in this plane. The 5σ a_1 orbitals lie so low in energy that they are in the energy range of the carbonyl's π-bonding orbitals. Weak interactions with the 1π orbitals cause the 5σ a_1 orbital to be distributed among two MO's shown in parts e and f of Figure 6. They are plotted in the *yz* plane to show the metal character in these orbitals; therefore, the bridging carbonyls' 5σ contribution, the principal contribution, is not observed. Both of these orbitals have a surprisingly large amount of metal character, with Figure 6e possessing some character from the $1a_1$ orbital of the $Co_2(CO)_6$ fragment and Figure 6f possessing some character from the $2a_1$ orbital. These orbitals may have enough metal–metal bonding character to provide a net bond between the cobalt atoms. Therefore, the three high-lying frontier orbitals, b_2, a_1, and a_2, together with the lower lying b_1 and a_1 orbitals from the carbonyls' 5σ orbitals are of the correct symmetry and could provide the five electron pairs necessary for four equivalent Co–C_{br} bonds and a Co–Co bent bond.

Fragment Deformation Density. In the theoretical deformation density studies of $Mn_2(CO)_{10}$ and $ClCCo_3(CO)_9$,[7] it was found that the use of promolecules or constituent fragments produces fragment deformation density maps that possessed enhanced accumulation in the metal–metal bonding region. The enhancement arises because attachment of the terminal ligands to the metal centers removes density from the metal–metal bonding regions relative to the spherical atom. In order to better describe the Co–Co interaction in $Co_2(CO)_8$, a fragment deformation density map could be computed in which the promolecule consists of the density of two isolated $Co(CO)_3$ fragments and two isolated CO molecules. The electronic structure of the $Co(CO)_3$ fragment and of the CO molecule used in the promolecule depends on how one constructs the model of the fragments before bonding to form $Co_2(CO)_8$.

If one wishes to model a promolecule for structure **1**, in which there is no direct Co–Co bond, there would be a doubly occupied d_π orbital in the *yz* plane at each Co atom in the molecule. This can be represented in the $Co(CO)_3$ fragment by doubly occupying the e orbital in the *yz* plane and singly occupying the remaining e orbital in the perpendicular *xy* plane. To complete the promolecule, the density of two isolated ground-state CO molecules are added to the density of the two doublet $Co(CO)_3$ fragments described above. The density of this promolecule is subtracted from the total molecular density to yield the "nonbonded" fragment deformation density maps shown in Figure 7.

Now let us consider a valence bond picture of $Co_2(CO)_8$, as shown in structure **2**, in which there are four equivalent Co–C_{br}

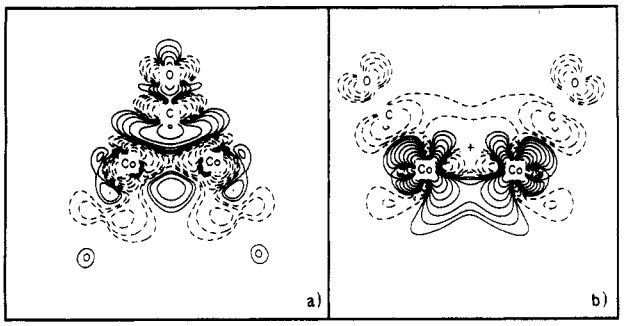

Figure 8. "Bonded" fragment deformation density maps using a promolecule consisting of the sum of the density of two quartet $Co(CO)_3$ fragments and an excited triplet state of a CO molecule with one electron from the 5σ orbital excited to the π^* orbital parallel to the Co–Co axis. The maps are shown in (a) the $Co_2(\mu\text{-}C)$ plane and (b) the yz plane. The contouring scheme is the same as in Figure 3.

bonds and a Co–Co bent bond. The $Co(CO)_3$ fragment would need to form hybrids derived from both e orbitals and the a_1 orbitals to give the needed three bonds from the Co atom. Therefore, the $Co(CO)_3$ fragments would have two e orbitals and the a_1 orbital would be singly occupied. Ideally, in order to complete the promolecule density for this arrangement, a "ketenyl" CO molecule is required in which one electron from the doubly occupied 5σ orbital in the ground-state CO molecule is promoted to the 2π orbital parallel to the Co–Co axis. The density of two ketenyl CO molecules plus two quartet $Co(CO)_3$ fragments is then subtracted from the total molecular density to form the "bonded" fragment deformation density maps, shown in Figure 8.

The nonbonded fragment deformation density is shown in the $Co_2(\mu\text{-}C)$ plane in Figure 7a and in the *yz* plane in Figure 7b. Since the density of the CO molecule was subtracted, the changes due to C–O bond formation are not observed in Figure 7a, only changes due to formation of the $Co–C_{br}$ bond. Therefore, Figure 7a shows density loss in the bridging carbonyl's σ region due to σ donation from the carbonyl to the cobalts and gain in the bridging carbonyl's π region due to π back-donation from the cobalts to the carbonyl. The density loss in the σ region and gain in the π region are much larger than that observed for terminal carbonyls.[25] The features about the Co atom show loss along the $Co–C_{br}$ axis presumably due to the π back-donation to the carbonyl. In Figure 7b, there is a definite accumulation peak in the bent-bond region. The doubly occupied e orbital in the fragment has lost density to the terminal carbonyls and to the bent bonding region. This can be attributed to the doubly occupied e orbital in the $Co(CO)_3$ fragments overestimating the density in the same orbitals in the molecule. Additionally, there is a large accumulation region near the cobalt atoms perpendicular to the Co–Co axis. This accumulation region is probably due to the interaction of the bridging carbonyls rearranging the nonbonded density on the $Co(CO)_3$ fragments.

The bonded fragment deformation density is shown in the $Co_2(\mu\text{-}C)$ plane in Figure 8a and in the *yz* plane in Figure 8b. In Figure 8a, in contrast to the nonbonded fragment deformation density (Figure 7a), there is now density accumulation in the bridging carbonyl's σ region and density loss in its π region. Although it is too extreme to view the bridging carbonyls as ketonic, both fragment deformation densities show that the bridging carbonyls do possess substantial ketonic character. The σ accumulation associated with the bridging carbonyl extends into the $Co–C_{br}$ internuclear region. In Figure 8b, a large accumulation region appears in the e_g-like orbital in this plane (*yz*). Additionally, a deficit region appears in the region of the a_1 hybrid orbital. These observations indicate that singly occupying both of these orbitals in the promolecule underestimates the molecular density in the e_g-like orbital and overestimates the density in the a_1 orbital. Once again, there is an accumulation region in the bend-bond region. However, whether this accumulation is due to Co–Co bonding or is simply an overlap of the accumulation in the cobalts' e_g-like orbital is hard to discern in these maps.

As shown from the extreme cases presented by the two promolecules utilized in the two fragment deformation density studies, the electronic structure lies somewhere between the nonbonding case of two doubly occupied d_π orbitals shown in **1** and the electron-pair bonding case as indicated by structure **2**. Additionally, the accumulation region in the bent-bond region in the nonbonded fragment deformation density maps in Figure 7b is indicative that there is at least some constructive interference between the cobalts. If the internuclear accumulation was due just to atomic orbital accumulations, there should not be an internuclear accumulation in Figure 7b where the density of the doubly occupied *yz* component orbital of the e″ set of the two $Co(CO)_3$ fragments is subtracted from the molecular density. The resultant accumulation between the Co atoms in this map must be due to expansion of the atomic orbitals toward the internuclear region or, in other words, constructive interference between the Co atoms.

Localized Orbitals. In order to examine the wave function of $Co_2(CO)_8$ in terms of a localized bonding picture, we attempted to localize the orbitals of $Co_2(CO)_8$ using the Boys criterion.[26] When all the orbitals are included in the localization, the orbitals localized into a bonding scheme as shown in **4**, in which there is

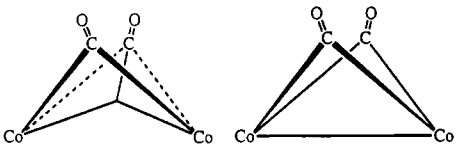

4 **5**

a 3-center 2-electron bond between the two cobalt atoms and one of the bridging carbonyls. There are also two orbitals that localize to two separate $Co–C_b$ bonds. On the opposite $Co_2(\mu\text{-}C)$ wing, two orbitals localize into two separate $Co–C_b$ bonds that are located closer toward the center of the molecule than the localized $Co–C_b$ bond orbitals on the other wing. In order to fully describe the system, the bonding shown by **4** should be considered to be one of two resonance forms of $Co_2(CO)_8$.

Since the molecular orbital associated with the Co–Co interaction is already fairly well localized (see Figure 5a), we decided to try to localize all the molecular orbitals except for the Co–Co bonding a_1 bonding orbital. In this case, the orbitals associated with $Co–C_b$ bonding all localized into four equivalent $Co–C_b$ bonds yielding a view of $Co_2(CO)_8$, as shown in **5**. Among the other localized orbitals, there are six localized orbitals that localize cleanly into six t_{2g}-like orbitals with three on each cobalt atoms. One of these six orbitals is plotted in the *yz* plane in Figure 9a. It can clearly be observed in this plot that most of this orbital is located on one of the cobalt atoms. One of the localized $Co–C_b$ orbitals is shown in the $Co_2(\mu\text{-}C)$ plane in Figure 9b and in the *yz* plane in Figure 9c. From these plots it can be seen that most of this orbital is located along the $Co–C_b$ axis but there is some character on the other cobalt atom. The interaction between the two cobalts appears to be essentially nonbonding.

From the results of the localization, it would seem that there is some direct Co–Co interaction present in $Co_2(CO)_8$. Even when all the orbitals are included in the localization, the resultant localized picture yields a 3-centered, 2-electron interaction between the two cobalts and one of the bridging carbonyls. This would indicate that the direct Co–Co interaction is intrinsically tied up with the bridging carbonyls. Whether this direct interaction between the cobalts is enough to produce a Co–Co bond in the analysis of the topology of the charge density is examined in the next section.

Topology of the Charge Density. The topology of the molecular charge density was studied to ascertain whether this analysis would yield a direct Co–Co bond. According to this analysis, if the

(25) Sherwood, D. E.; Hall, M. B. *Inorg. Chem.* **1983**, *22*, 93.

(26) Foster, J. M.; Boys, S. F. *Rev. Mod. Phys.* **1960**, *32*, 300.

Table I. Analysis of the Topology of the Charge Density of $Co_2(CO)_8$

Atomic Positions

atom	position			atom	position		
Co	0.0000	±2.3896	−0.0494	O_{t1}	0.0000	±5.4949	4.5894
C_b	±2.5104	0.0000	1.1400	C_{t2}	±2.5093	±3.7478	−2.0099
O_b	±4.5033	0.0000	2.0842	O_{t2}	±4.0640	±4.5893	−3.2245
C_{t1}	0.0000	±4.2986	2.8024				

Critical Points

atoms	position			type	eigenvalues (λ_1, λ_2, λ_3)		
			Without Bond Center Basis Functions				
Co–Co	0.0000	0.0000	0.1365	(3,+1)	−0.0110	0.0430	0.0856[a]
Co–C_b	±1.3018	±1.2867	0.5601	(3,−1)	−0.1290	−0.1258	0.5476
$(CO)_b$	±3.2114	0.0000	1.4710	(3,−1)	−1.2269	−1.1953	3.1654
Co–C_{t1}	0.0000	±3.3663	1.3931	(3,−1)	−0.1865	−0.1832	1.0313
$(CO)_{t1}$	0.0000	±4.7207	3.4323	(3,−1)	−1.4548	−1.4546	3.9132
Co–C_{t2}	±1.2193	±3.0358	−1.0108	(3,−1)	−0.1264	−0.1123	0.9464
$(CO)_{t2}$	±3.0596	±4.0443	−2.4376	(3,−1)	−1.4813	−1.4784	3.9747
			With Bond Center Basis Functions				
Co–Co	0.0000	0.0000	0.3092	(3,+1)	−0.0222	0.0614	0.0719[a]
Co–C_b	±1.3018	±1.2867	0.5601	(3,−1)	−0.1293	−0.1228	0.5473
$(CO)_b$	±3.2116	0.0000	1.4769	(3,−1)	−1.2291	−1.1974	3.1620
Co–C_{t1}	0.0000	±3.3659	1.3994	(3,−1)	−0.1866	−0.1838	1.0309
$(CO)_{t1}$	0.0000	±4.7207	3.4382	(3,−1)	−1.4548	−1.4546	3.9132
Co–C_{t2}	±1.2190	±3.0357	−1.0051	(3,−1)	−0.1262	−0.1122	0.9467
$(CO)_{t2}$	±3.0596	±4.0443	−2.4136	(3,−1)	−1.4813	−1.4784	3.9747

[a] The eigenvalues for the (3,+1) critical point between the Co atoms point along the z axis, the x axis, and the y axis in that order.

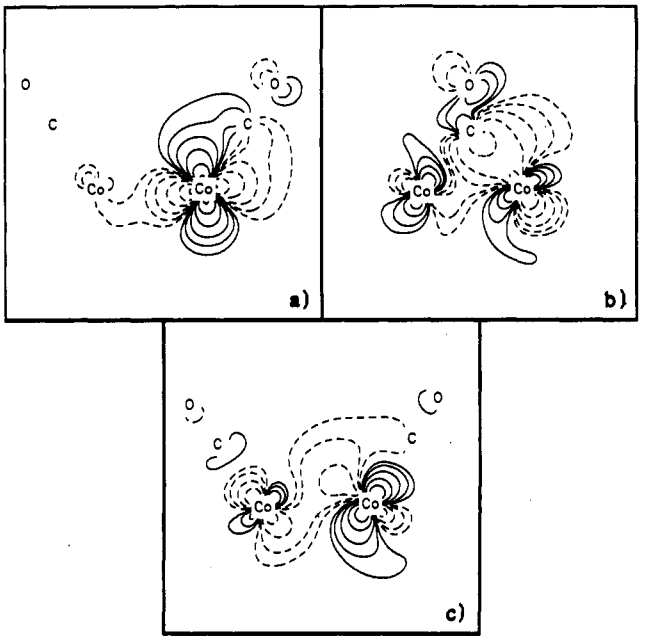

Figure 9. Molecular orbital plots of selected localized orbitals of $Co_2(CO)_8$ from the second localization of $Co_2(CO)_8$ (all valence orbitals except Co–Co a_1 bonding orbital localized): (a) a t_{2g}-like orbital localized on one of the Co atoms in the yz plane; (b) one of the localized Co–C_b bond orbitals in the $Co_2(\mu$-C) plane; (c) same as (b) except in the yz plane. Plots are contoured as in Figure 6.

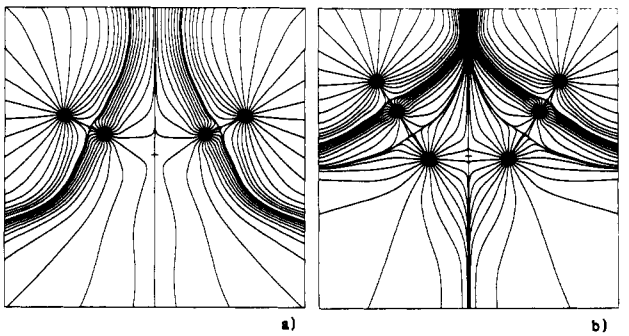

Figure 10. Gradient vector field of ρ for $Co_2(CO)_8$ in the two symmetry planes of the molecule: (a) xz plane containing the two bridging carbonyls, (b) yz plane containing the two cobalt atoms and the axial terminal carbonyls. The (3,+1) critical point between the cobalt atoms is denoted by a hatch mark on the boundary line down the middle of both plots. The (3,−1) critical points are denoted by a "x" along the bond paths.

electronic structure of $Co_2(CO)_8$ possessed a Co–Co bond, there would be a (3,−1) critical point between the cobalt atoms and between all other bonded atoms. Additionally, there would be a (3,+1) ring critical point somewhere in each of the $Co_2(\mu$-C) rings. However, if the electronic structure of $Co_2(CO)_8$ is more like **1** without a direct Co–Co bond, there would be no (3,−1) critical point between the cobalt atoms. The only critical point that could exist between the cobalt atoms would be a (3,+1) ring critical point that would exist inside the $Co_2(\mu\text{-C})_2$ ring.

The critical points of the gradient of the density of $Co_2(CO)_8$ are listed along with the eigenvalues of the Hessian matrix (λ_1, λ_2, λ_3) in Table I. λ_1 and λ_2 are the eigenvalues in the direction perpendicular to the atom–atom axis, and λ_3 is the eigenvalue parallel to the interatomic axis. Note that a (3,+1) critical point exists between the cobalt atoms. It lies on a point slightly above the Co–Co axis toward the bridging carbonyls. The values of the eigenvalues perpendicular to the cobalt–cobalt axis (λ_1, λ_2) are relatively small compared to the same values for the (3,−1) critical points. The gradient vector fields of $Co_2(CO)_8$ are shown in the two planes of symmetry in Figure 10, the yz plane in Figure 10a and the xz plane in Figure 10b.

Because of the small value of the perpendicular eigenvalues at the Co–Co (3,+1) critical point, it might be proposed that the use of a larger basis set might be enough to change this critical point into a (3,−1) bond critical point between the cobalts. To test this hypothesis, a set of bond-centered basis functions were added to the previous basis set (two s functions of exponents 3.6 and 1.2 and one p function of exponent 2.0), which were located at the Co–Co midpoint. If the inclusion of bond-centered basis functions does not alter the topology of the charge density between the cobalt atoms, it is unlikely that any further enlargement of the atomic basis set could alter it. The resultant critical points and their corresponding eigenvalues are listed in the second part of Table I. As can be observed, the inclusion of the bond-centered basis functions does not change the overall topology of the

molecule. In fact, the value of the smallest positive perpendicular eigenvalue, λ_2, actually increases.

Ab initio SCF calculations on the isolobal complex $[(\eta^5\text{-}C_5H_5)Co(\mu\text{-}NO)]_2$, which experimentally possesses a much smaller Co–Co separation of 2.372 (1) Å,[27] yield a (3,-1) bond critical point between the Co atoms.[28] In order to observe how the topology of the density of $Co_2(CO)_8$ changes with a shorter Co–Co separation, the SCF calculation was performed with a Co–Co separation of 2.37 Å. The density of this geometry of $Co_2(CO)_8$ now possesses a (3,-1) bond critical point between the Co atoms. This critical point is located 0.02 Å "below" the Co–Co axis opposite the bridging carbonyls. The values of the perpendicular eigenvalues for this critical point are quite small at -0.0267 and -0.00833. This behavior is an indication of the flat nature of the charge density inside the $Co_2(\mu\text{-}C)_2$ ring. The density need not change much to alter the nature of the critical point between the cobalt atoms.

Conclusions

According to the topology of the charge density alone, there is no direct Co–Co bond in $Co_2(CO)_8$. All of the formal bonds between the two cobalt atoms occur through the bridging carbonyls. Therefore, the accumulations observed in the bent-bond regions of both the standard deformation density and the fragment deformation density maps are not sufficient to produce enough concentration of density between the cobalt atoms to form a bond.

However in the "nonbonded" fragment deformation density, the d_{yz} orbitals in each $Co(CO)_3$ fragment in the promolecule are already doubly occupied. So the accumulation in the Co–Co "bent-bond" region is most likely due to constructive interference between the two cobalt d_{yz} fragment orbitals. If one compares the standard deformation densities of the bridged and unbridged isomers, it could be suggested that if the unbridged isomer has a single Co–Co bond, then the bridged isomer has a bond order of $^1/_3$. However, this weak Co–Co interaction is not sufficient to alter the topology of the charge density enough to produce a (3,-1) bond critical point between the cobalt atoms.

Because the density and its derivatives are 1-electron properties, one would expect our results to be relatively stable with respect to the changes in the wave function introduced by electron correlation. We have carried out some preliminary configuration interaction calculations on $Co_2(CO)_8$[29] and more extensive calculations on the isolobal $Cp_2Co_2(NO)_2$.[28] Basically, in $Co_2(CO)_8$ the correlated wave function is strongly dominated by the single-determinant HFR configuration. In these situations previous results have shown that the density and its derivatives are qualitatively left unchanged by the addition of electron correlation.[30]

Registry No. $Co_2(CO)_8$, 10210-68-1.

(27) Bernal, I.; Korp, J. D.; Reisner, G. M.; Hermann, W. A. *J. Organomet. Chem.* **1977**, *139*, 321.
(28) Low, A. A.; Hall, M. B. To be submitted for publication in *Inorg. Chem.*
(29) Kunze, K. L.; Hall, M. B. Unpublished results.
(30) Gatti, C.; MacDougall, P. J.; Bader, R. F. W. *J. Chem. Phys.* **1988**, *88*, 3792.

Contribution from the Department of Chemistry and Materials Science Center, Cornell University, Ithaca, New York 14853, and Departament de Quimica Inorgânica, Universitat de Barcelona, Diagonal 647, Barcelona 08028, Spain

Electronic Structure of a $[Tc_2(\mu\text{-}O)_3Cp]_n$ Polymer with a Very Short Metal–Metal Bond

A. W. Edith Chan,[†] Roald Hoffmann,*[,†] and Santiago Alvarez[‡]

Received May 18, 1990

This recently synthesized polymer (with C_5Me_5) has a very short Tc–Tc distance of 1.867 Å. Its electronic structure is discussed by using molecular models and band calculations. The net bonding in a model $CpTcO_3TcCp^-$ is best described qualitatively as $\sigma^2(\pi\delta)^4\delta^*$, i.e. a net bond of approximate order 2.5. The details of the polymer's electronic structure are consistent with this. While bonding in multiply bridged dimers or polymers is never easy to sort out, we think the short Tc–Tc bond is consonant with a multiple metal–metal bond superimposed on an already short Tc–Tc contact enforced by the three bridging oxygens.

Recently, a polymeric compound with an extremely short technetium–technetium distance, $[Tc_2(\mu\text{-}O)_3(C_5Me_5)]_n$, was reported.[1] The unusually short metal–metal bond (1.867 Å) and the 3.5+ formal oxidation state of each Tc clearly suggest a multiple bond between the two metals. Around 20 Tc dimers have been synthesized in the past 20 years.[2] The Tc–Tc distances in these usually range from 2.05 to 3.14 Å. Many of these dimers are supported by bridging ligands, and only a few are held together by a direct metal–metal bond. Typical of these is quadruply bonded $Tc_2Cl_8^{2-}$, which has a Tc–Tc bond length of 2.14 Å.[3] The shortest previously reported Tc–Tc separation is 2.05 Å, in $Tc_2Cl_6^{2-}$.[4] So the much shorter bond in the Kanellakopulos and Ziegler polymer is truly striking. While supershort Cr–Cr bonds exist, and are quite well understood, there is no obvious rationale for the unusually short Tc–Tc distance in this polymer. Our study explores the bonding in this molecule, probing the nature of the metal–metal bond in it, and the role of the bridging oxygens. It should be noted that the Tc_2O_3Cp structure has been questioned;[5] there is a real scientific argument brewing. Whichever way it is resolved, i.e. whether the structure of the polymer is correct or not, it is interesting to think about such a chain and its bonding.

Structure **1** shows a view of the polymer. In molecules where a metal–metal bond is bridged by other ligands, it has never been

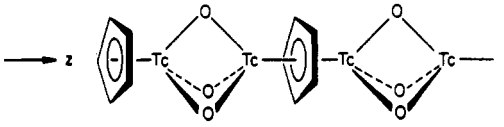

1

easy to sort out direct metal–metal bonding from bridging. One

(1) Kanellakopulos, B.; Nuber, B.; Raptis, K.; Ziegler, M. L. *Angew. Chem.* **1989**, *101*, 1055; *Angew. Chem., Int. Ed. Engl.* **1989**, *28*, 1055.
(2) (a) Bailey, M. F.; Dahl, L. F. *Inorg. Chem.* **1965**, *4*, 1140. (b) Bratton, W. K.; Cotton, F. A. *Inorg. Chem.* **1970**, *9*, 789. (c) Cotton, F. A.; Gage, L. D. *Nouv. J. Chim.* **1977**, *1*, 441. (d) Cotton, F. A.; Fanwick, P. E.; Gage, L. D. *J. Am. Chem. Soc.* **1980**, *102*, 1570. (e) Bürgi, H.-B.; Anderegg, G.; Bläuenstein, P. *Inorg. Chem.* **1981**, *20*, 3829. (f) Cotton, F. A.; Davison, A.; Day, V. W.; Fredrich, M. F.; Orvig, C.; Swanson, R. *Inorg. Chem.* **1982**, *21*, 1211. (g) Colmanet, S. F.; Mackay, M. *J. Chem. Soc., Chem. Commun.* **1987**, 705. (h) Anderegg, G.; Müller, E.; Zollinger, K. *Helv. Chim. Acta* **1983**, *66*, 1593. (i) Linder, K. E.; Dewan, J. C.; Davison, A. *Inorg. Chem.* **1989**, *28*, 3820.
(3) Cotton, F. A.; Daniels, L. *Inorg. Chem.* **1981**, *20*, 3051.
(4) Kryutchkov, S. V. *Dokl. Akad. Nauk. SSSR* **1986**, *288*, 389.
(5) Herrmann, W. A.; Alberto, R.; Kiprof, P.; Baumgärtner, F. *Angew. Chem.* **1990**, *102*, 208; *Angew. Chem., Int. Ed. Engl.* **1990**, *29*, 189.

[†] Cornell University.
[‡] Universitat de Barcelona.

0020-1669/91/1330-1086$02.50/0